Microscopic origins of the surface exciton photoluminescence peak in ZnO nanostructures

Mahua Biswas,[1,*] Yun Suk Jung,[2] Hong Koo Kim,[2] Kumarappan Kumar,[3] Gregory J. Hughes,[3] S. Newcomb,[4] Martin O. Henry,[1] and Enda McGlynn[1]

[1]*School of Physical Sciences, National Centre for Plasma Science and Technology, Dublin City University, Glasnevin, Dublin 9, Ireland*

[2]*Department of Electrical and Computer Engineering, Petersen Institute of NanoScience and Engineering, University of Pittsburgh, Pittsburgh, Pennsylvania 15260, USA*

[3]*School of Physical Sciences, National Centre for Sensor Research, Dublin City University, Glasnevin, Dublin 9, Ireland*

[4]*Glebe Scientific Ltd., Newport, Co. Tipperary, Ireland*

(Received 10 September 2010; revised manuscript received 4 April 2011; published 13 June 2011)

We report photoluminescence (PL) studies of the surface exciton peak in ZnO nanostructures at ∼3.367 eV aimed at elucidation of the nature and origin of the emission and its relationship to the nanostructure morphology. PL spectra in conjunction with localized voltage application in high vacuum and different gas atmospheres show a consistent variation (and recovery), allowing an association of the PL to a bound excitonic transition at the ZnO surface, which is modified by an adsorbate. PL studies of samples treated by plasma and of samples exposed to UV light under high vacuum conditions, both well-known processes for desorption of surface adsorbed oxygen, show no consistent effects on the surface exciton peak indicating the lack of involvement of oxygen species. X-ray photoelectron spectroscopy data strongly suggest involvement of adsorbed OH species. X-ray diffraction, scanning, and transmission electron microscopy data are presented also, and the relationship of the surface exciton peak to the nanostructure morphology is discussed.

DOI: 10.1103/PhysRevB.83.235320 PACS number(s): 78.55.Et, 81.07.−b, 71.35.−y, 68.43.−h

I. INTRODUCTION

ZnO nanostructures provide an ideal system to study the influence of surface effects on optical properties due to their large surface-to-volume ratios. Photoluminescence (PL) studies of bulk and nanostructured ZnO material reveal a range of near band-edge excitonic emission lines, mostly donor bound exciton (DBE) lines, at low temperature, denoted by the labels I_0 to I_{11},[1] which are visible in both bulk and nanostructured ZnO samples. However, an asymmetric peak, broader than the I lines (∼5 meV), at ∼3.367 eV, denoted as I_2 by Meyer *et al.*[1] and as a surface-related bound exciton (SX) peak by various authors, can be seen also, mostly in nanostructured materials.[2–7] This was observed in freshly cleaved ZnO crystals by Travnikov *et al.*[8] and more recently only in emission from ZnO nanostructures with high surface-to-volume ratios.[2,3,5,6,9,10] These properties, and the parallels with similar emissions observed in a range of other materials,[4,11–14] have led to its labeling as a bound exciton transition at a surface or near surface defect. This peak has been studied by the ZnO community with increasing interest due to its association with surface-related phenomena, which are important issues for applying nanostructures in, e.g., optical devices.[2,5,7–10,15,16] Although the SX peak itself is visible only at temperatures below 25 K, nanostructures showing the SX peak also have rapidly decaying band-edge intensity with increasing temperature,[7] and it appears that the surface conditions responsible for the SX peak lead also to temperature-activated nonradiative recombination processes at higher temperatures.

Evidence for the surface nature of the defect responsible has come from studies of the scaling of relative peak intensity with experimental conditions and nanostructure morphology,[2,6,10,17] and the inhomogeneously broadened line shape was concluded to be due to bound excitons (BE) with either different distances to the surface or differences in interaction with additional surface centers of an inhomogeneous nature (such as reconstructions, dangling bonds, impurities, etc.), similar to the case of CdS.[2,11–13] Richters *et al.*[5,9] reported a significant increase in the SX peak intensity in polymer-coated ZnO nanowires and ZnO/Al_2O_3 core-shell nanowires compared to as-grown ZnO nanowires and explained their data in terms of the polymer/Al_2O_3 layers acting as a screening dielectric medium. Voss *et al.* have reported the effects of metal coatings that reduce the SX peak relative intensity, which was explained in terms of metal-induced gap states.[18]

The reports above provide evidence for the surface nature of the SX peak emission, but a number of gaps in understanding remain, including whether the defect(s) responsible are crystal defects confined to the (sub-) surface region[19] or adsorbed surface species that can bind excitons in their vicinity. Adsorption and/or chemisorption processes at semiconductor surfaces, and specifically in the case of ZnO, are reasonably well known, and species such as O_2^-, O^-, O^{2-}, OH^-, H_2O, etc., are common adsorbates at the surface of ZnO.[20–22] Adsorbates such as these have been considered previously as possible origins of the SX band,[5,6,9,16] with particular attention on O and O_2, but no conclusion has been reached. Also, the assignment of the large surface-to-volume ratio of nanostructures as the sole or main determinant of the SX peak relative intensity is questionable given the existence of a number of reports of low-temperature PL from ZnO nanostructures with varying aspect ratios, which show no consistent correlation from one report to another between the SX peak relative intensity and the nanostructure aspect ratio (as well as variations with morphology variations seen within individual reports); see e.g., Refs. 17 and 23–25.

In this work, we study the effect on the SX peak intensity of localized voltage application in high vacuum and different gas atmospheres. We also study the effects on the SX peak of desorbing surface oxygen species using different

surface treatments including well-established methods such as plasma treatment and UV exposure under high vacuum conditions. X-ray photoelectron spectroscopy (XPS) studies of UV-illuminated samples have been done in the O 1*s* spectrum region before and after UV illumination to study the surface-adsorbed species. The effects of nanostructure morphology and crystallinity have been studied using x-ray diffraction (XRD) and scanning and transmission electron microscopy (SEM and TEM, respectively) studies. Based on all these data, we conclude that the origin of the peak is due to a transition at an exciton bound at ZnO surfaces modified by adsorbed OH, and that the detailed morphology of the ZnO nanostructures is important in determining the intensity of the SX signal.

II. EXPERIMENTAL

The ZnO nanostructure growth technique is described in detail elsewhere.[26,27] Briefly, ZnO nanostructures were grown on Au-catalyzed *a*-plane (11-20) sapphire substrates and *n*-type (resistivity 2.5–8 Ω cm) and *p*-type (resistivity 5–9 Ω cm) Si substrates using vapor phase transport (VPT). A 5 nm Au layer was evaporated onto 5-mm-diam circular or 9-mm^2-square continuous areas on the ultrasonically cleaned substrates using a thermal evaporator. The furnace temperature is set at either 900 or 950 °C and samples were grown for 60 min.

PL spectra have been acquired using a Bomem DA8 FT spectrometer with the samples in a closed-cycle cryostat (Janis Research). All PL spectra in this study were taken with the same instrumental setup. The detector aperture enabled a spectral resolution of 5 cm^{-1} (∼0.4 meV). In all spectra, the SX peak has been compared to the other two main peaks (I_6 and I_9) in terms of peak intensity (not integrated intensity) since spectral linewidths were largely unchanged for all features.

Electrical voltages in vacuum, air and pure He atmospheres have been applied *in situ* in the cryostat sample chamber (to avoid, insofar as possible, adsorption of species from ambient during transfer from one chamber to another) via the temperature controller feed-through of the cryostat. Samples used for this study were grown on Si and an insulating 500 nm SiO_2 layer was deposited on the Si using plasma-enhanced chemical vapor deposition (PE-CVD) before ZnO deposition. A wire was attached to the ZnO nanostructure deposition area using an ∼2 mm pad of conductive Ag paste and another at the back of the sample on the Si (at ground potential). Voltages were applied for 1 h and the leakage current level varied in the range 10–20 mA. Both *n*- and *p*-type Si were used and both positive and negative voltages were applied to the nanostructures ranging from 40 to 70 V. Changes in the SX peak intensity were seen only from 50 V upward. At 70 V and above, the samples were damaged due to breakdown of the SiO_2 layer. Following voltage application, low temperature PL data were taken from regions adjacent (at a distance of ∼2 mm) to the electrical contact region in the ZnO nanostructure deposition area, with the sample always cooled in a He atmosphere.

The effects of a variety of surface treatments on the SX line intensity were studied. Plasma treatments were undertaken using both O and Ar plasmas. The O plasma was produced with an inductively coupled plasma reactive ion etching (ICP-RIE) system (Unaxis 790 ICP-RIE) with an ICP power of 125 W and an RIE power of 5 W, O pressure of 15 mTorr, and a flow rate of 30 sccm for 30 min. Two independent RF sources were used in this ICP-RIE system—one (ICP power) was inductively coupled to a low-pressure gas creating a high-density plasma, and another (RIE power) was applied to a sample chuck to produce a substrate bias that can extract and accelerate the reactive species from the plasma to the sample. The separate RF sources allowed independent control of ion density and energy. The Ar plasma was produced using the same instrument and conditions except the ICP power and time were reduced to 50 W and 5 min, respectively. In both plasmas, the RIE power was maintained at the minimum level to alleviate possible plasma damage to the ZnO samples. The ZnO nanostructures were exposed to the plasma without intentional heating of the sample.

UV illumination experiments were usually performed on the sample in the cryostat (similar to electrical voltage experiments) using a 250 W iron-doped metal halide UV lamp (UV-H 253 BL–UV Light Technology Ltd.). Samples were also illuminated in the XPS chamber described later. The spectral output of the lamp is from 280 to 450 nm (4.42 to 2.75 eV), and thus had a significant fraction (∼1/2) of photons with energy above the room-temperature band gap of ZnO (∼3.3 eV). PL spectra were taken before illumination and the temperature was then raised to room temperature and the sample chamber of the cryostat evacuated to $\sim 10^{-6}$ mbar (3×10^{-6} mbar is the lowest pressure the cryostat used can attain). The samples were illuminated for a range of times (6, 8, 20, and 24 h), and power densities of ∼22, 15, and 3 mW/cm^2 were obtained with a power meter at distances, respectively, of 0 cm (i.e., lamp directly touching meter), 3.5 cm (the sample distance within PL chamber), and 18 cm (the sample distance within the XPS chamber) from the lamp. The samples were then cooled to low temperatures to judge the effects on the SX PL peak.

Material surface composition before and after UV illumination were studied using XPS at base pressures in the preparation and analysis chambers of 2×10^{-6} and 1×10^{-9} mbar, respectively, using an Al $K\alpha$ ($h\nu$ = 1486.6 eV) x-ray source. The pass energy of the analyzer was set at 20 eV, yielding a resolution of approximately 1.0 eV. Binding-energy scale calibration was performed with the C 1*s* line (285 eV) from the adventitious carbon contamination layer.[28] The XPS peaks were fitted with a mixed ratio of Gaussian and Lorentzian line shapes and a Shirley background function.

SEM images were taken using a field-emission SEM (FESEM) system (Hitachi S-4300 field emission system) and a LaB_6 emitter system (Karl-Zeiss EVO series). XRD was performed using a Bruker AXS D8 advance texture diffractometer. TEM studies were performed using a JEOL2000FX system operating at 200 kV. TEM specimens were prepared either by mechanically scraping nanorods from the substrate onto a TEM grid, or using standard focused ion beam thinning (FEI FIB 200 workstation operating at 30 kV using a Ga ion source with currents of 11 nA and 150 pA for box milling and final polishing, respectively).

III. RESULTS

A. SX peak behavior after electrical voltage application

In Figs. 1(a)–1(c), PL spectra for samples where voltages of 60 V were applied in vacuum are shown. For voltages of 50 V, the same changes as shown in Figs. 1(a)–1(c) have been observed (data not shown). From Fig. 1(b) it is observed that the SX peak relative intensity has increased significantly compared to the *I*-line peaks after voltage application. The notable point is that the SX peak relative intensity dropped down again to its initial value after exposure to air, as shown in Fig. 1(c). These data were consistently reproducible on a large number of samples. Also, no differences were seen for experiments with positive and negative applied biases in vacuum—for both biases the change and recovery of the SX peak was identical.

PL spectra for samples where voltages of 60 V were applied in air and He are shown in Figs. 1(d)–1(f) and 1(g)–1(i), respectively. All of the experiments in air and He used a fixed positive voltage of 60 V. These experiments again show consistent and reproducible results with significant and differing responses of the SX peak intensity to the applied voltage in different atmospheres. After voltage application in air, the relative intensity of the SX peak has decreased [Fig. 1(e)], and after reexposure to ambient the SX peak increases again and returns to its initial level, as shown in Fig. 1(f). After voltage application in He, shown in Fig. 1(h), the relative intensity of the SX peak remains identical to that before voltage application shown in Fig. 1(g), and after reexposure to ambient it remains unchanged [Fig. 1(i)]. We note that in all cases following voltage application, the changes in the PL spectra remain after the voltage is turned off and the sample electrical connections grounded. The spectra only recover to their prevoltage application levels when actually reexposed to air over time scales of at least 12 h.

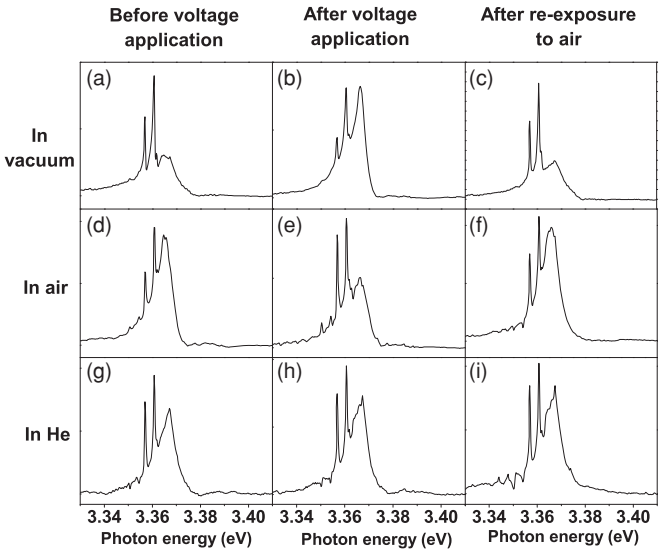

FIG. 1. PL study by voltage (60 V) application in vacuum (a)–(c), air (d)–(f), and He gas (g)–(i). (a), (d), and (g) are PL spectra taken at 18 K before voltage application; (b), (e), and (h) are PL spectra taken at 18 K after voltage application; and (c), (f), and (i) are PL spectra taken at 18 K after reexposure to air without voltage, respectively (PL intensity scales are linear).

The samples used in Figs. 1(a)–1(i) were grown on *p*-type Si substrates, and no differences in the SX relative intensity are seen for measurements made on samples grown on *n*-type Si substrates compared to those grown on *p*-type Si substrates (data not shown).

B. SX peak behavior after plasma treatment

Plasma treatments with both O and Ar plasmas were performed on ZnO nanostructure samples grown on *a*-sapphire at 900 °C. Initially, O plasma was used to treat nanostructured samples. Later in the study, Ar plasma was used to treat subsequent nanostructured samples to utilize an O-free plasma source.

From the FESEM image in Fig. 2(a) of a sample treated with the O plasma, we can see the nanorods were physically damaged during the plasma treatment and almost all the nanorods and some nanowalls were displaced from the substrate. However, the PL spectra in Figs. 2(c) and 2(d) show no significant change in the SX peak compared to the other *I*-line peaks. There are some slight changes in the spectral shape, especially at the higher photon energies where the surface treatment may have affected the free-exciton polariton properties and escape probability, but the overall relative intensity at the SX peak region has hardly changed, and in fact it has increased slightly. An Ar plasma treatment was undertaken next, and to eliminate or reduce nanorod damage, the ICP power was reduced to 50 W from 125 W while keeping the RIE power at the minimum level (5 W), and with the treatment time reduced to 5 min from 30 min. From the FESEM images of the sample in Fig. 2(b), we observe that in this experiment the damage to the nanorods is much less than that seen in the O plasma treatment, but nevertheless some nanorods are still physically displaced. The PL spectrum after plasma treatment in Fig. 2(f) shows no significant decrease in the SX peak intensity compared to the as-grown sample spectra in Fig. 2(e), although again we see a decrease in signal at the higher photon energies where the surface treatment may have affected the free-exciton polariton properties. Both of these observations show that the lower power Ar plasma treatment has affected the samples. In this case, we also observe that the I_9 peak decreases compared to other spectral features. We believe that the change in I_9 (In-related) peak intensity may be related to the preferential surface aggregation of in ZnO nanostructures proposed by Fan *et al.*,[19] which could be disproportionately affected by certain surface treatments.

C. SX peak behavior after UV illumination

PL spectra of four sets of experiments are shown below in Fig. 3 comprising sets of data from four different samples grown on *a*-sapphire at 900 °C taken using illumination times of 6, 8, 20, and 24 h (shown from the first row to the fourth row in Fig. 3, respectively). The vertical columns from left to right show the PL spectra before illumination, after illumination, and after air exposure, respectively, and data for the same sample are on a single row. The broad peak at ∼3.367 eV in

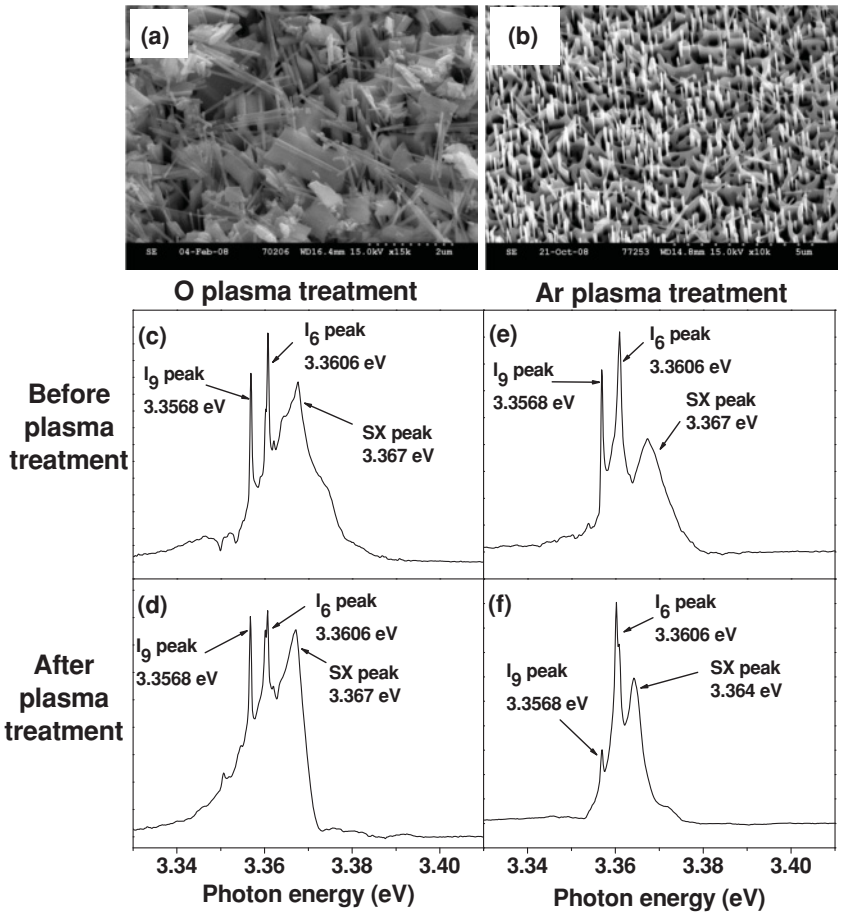

FIG. 2. (a) and (b) FESEM images of O and Ar plasma treated sample, respectively, after plasma treatment; (c) and (d) PL spectra at 18 K of the sample shown in (a) before and after O plasma treatment, respectively. (e) and (f) are the PL spectra of the sample at 18 K shown in (b) before and after Ar plasma treatment, respectively (PL intensity scales are linear).

all spectra in Fig. 3 is the SX peak. For the 6 h illumination period, we can see the relative intensity of the SX peak is almost the same [Fig. 3(b)], while for 8 and 20 h illumination this peak intensity increases [Figs. 3(e) and 3(h), respectively] after UV light illumination. For 24 h illumination, the SX peak intensity is almost the same in all spectra, but the linewidth has narrowed slightly after UV illumination [Fig. 3(k)].

After UV illumination and measurement, these samples were taken out to air (for a minimum of 12 h in all cases), and the PL spectra were then measured again. There is no evidence of significant changes after exposure to air, although the 6 h illuminated sample shows a slight increase in SX peak intensity [Fig. 3(c)]; in the case of the 8 and 20 h illuminated samples, the SX peak intensity decreased slightly [Figs. 3(f) and 3(i), respectively]; for the 24 h sample, the SX peak intensity was almost identical to that before exposure to air [Fig. 3(l)]. Further experiments have been done using post-illumination exposure to pure O_2 gas, rather than air, and in all cases the SX peak intensity is almost identical to that before exposure to O_2 (i.e., the same result as shown in the third column of Fig. 3).

D. XPS study of UV-illuminated samples

XPS studies of ZnO nanostructure samples showing intense SX peaks in PL were undertaken, and specifically the XPS spectra were taken before UV illumination and after UV illumination in ultra-high vacuum ($\sim 10^{-9}$ mbar) within the XPS chamber to investigate any surface compositional changes. The sample was kept inside the XPS chamber during illumination, and the power density at the sample (18 cm from the UV source) was ~ 3 mW/cm^2, as mentioned previously. The XPS O 1*s* spectra before and after illumination display a clear multipeak structure as shown in Fig. 4, whereas the Zn $2p_{3/2}$ spectra do not show much structure or differences from measurement to measurement (data not shown).

It has always been observed in XPS studies of various ZnO samples that the O peak is more sensitive to compositional changes compared to the Zn peak,[29] hence we concentrate on the O region of the spectrum. The detailed peak fittings of the O 1*s* spectra are shown in Fig. 4, and they indicate that the peak profile is consistent with the observation of four component peaks, two of which are ZnO-related, one an SiO_2-substrate related signal, and one a carbon-bonded oxygen component. In all the fits, the chemical shifts between the three main O 1*s* components have been held constant, and the energy difference between the Si-O peak of the O 1*s* region and the oxidized Si 2*p* peak (data in this region not shown) has been confirmed to remain constant and equal to the literature value.[30,31] Furthermore, the peak widths were allowed to vary in the fitting but were found in all cases to be very consistent and equal to 1.5 ± 0.1 eV, similar to data taken from ZnO planar samples. Care was taken to place the sample in as close to identical a position under the x-ray beam after each UV illumination as possible. However, because the ZnO grew on 9 mm^2 square Au islands and the x-ray beam illuminated the bare Si/SiO_2 beside the ZnO deposit, slight changes in translational and/or angular position upon repositioning could lead to differences in the

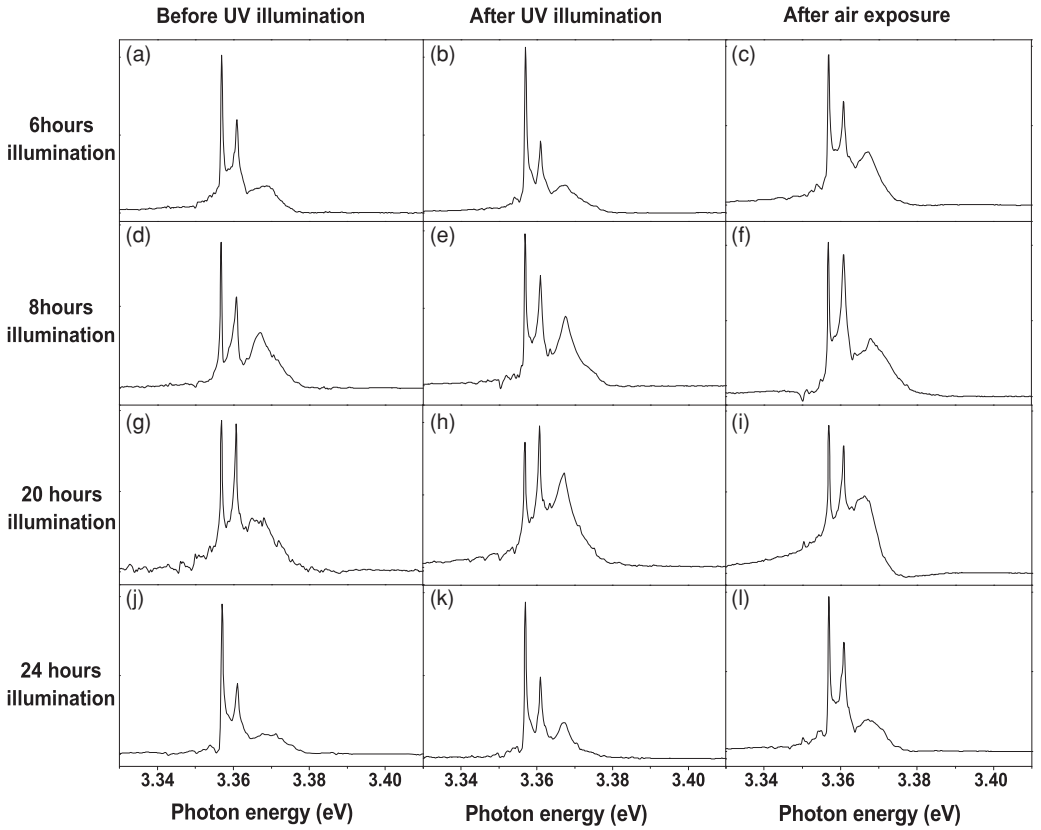

FIG. 3. PL spectra (at 18 K) of ZnO nanostructure samples illuminated with UV light for different time durations. Illumination time: (a)–(c) 6 h, (d)–(f) 8 h, (g)–(i) 20 h, and (j)–(l) 24 h (PL intensity scales are linear). The first column indicates the spectra before illumination, the second column after illumination, and the third column after reexposure to air (post-UV illumination).

amount of bare SiO_2 substrate illuminated from measurement to measurement; this would have an impact on the contribution of this component peak to the overall O 1*s* profile as mentioned below. The O 1*s* component peak at 531 eV is attributed to the lattice oxygen in ZnO, in agreement with the literature,[32] while the hydroxide peak (ZnOH) is shifted by 1.5 eV (Refs. 33 and 34) to higher binding energy. Neither of these peaks, nor their relative intensities, are significantly changed as a result of the UV radiation treatment, even though a small increase in the intensity of the OH-related component peak has been reported by other groups[35–37] after UV irradiation, attributed to the desorption of O/O_2 species from the ZnO surface, which subsequently react with residual water vapor to form OH groups on the surface. The signal at ∼533.3 eV in the O 1*s* region is attributed to O bonded as SiO,[30,31] due to the SiO_2 native oxide on the substrate regions not covered by Au and ZnO. This peak shows a substantial variation in intensity, but this correlates with intensity changes seen in the Si 2*p* region and is probably due to slight differences in the amount of the Si substrate illuminated from measurement to measurement as mentioned above. While this substrate-derived component peak complicates the analysis and makes it difficult to compare the exact percentage change of the surface-adsorbed O from peak fitting, it does not detract from the main observation that little change is observed in the ZnOH-related feature as a function of UV irradiation.

E. Correlation of SX peak intensity to nanostructure morphology and crystal quality

Figures 5(a)–5(d) show SEM and PL spectra of ZnO nanorod-nanowall and nanorod samples grown at 900 and 950 °C, respectively. The data from these two samples, and similar data from many other samples grown at 900 and 950 °C in our laboratory,[7] have helped us form a general conclusion about the relationship between the SX peak intensity at ∼3.367 eV in low-temperature PL and the ZnO nanostructure morphology. For growth at 900 °C, we always observe nanorod-nanowall morphology, and for growth at 950 °C, a nanorod morphology is almost always observed with the occasional presence of some short basewalls or sidewalls. From Figs. 5(a) and 5(b) we can see that, for the nanorod-nanowall morphology (where the diameters of nanorods are in the range of ∼95 nm and their lengths are in the range of ∼500 nm), an intense and broad SX peak is observed, which can occasionally overlap with free-exciton emission. From Figs. 5(c) and 5(d) we see that, for the nanorod-only morphology (i.e., mostly nanorods, occasionally with some short walls at the base of nanorods), the SX peak intensity is quite low, almost at the limit of detection. The diameter of nanorods for the 950 °C sample is similar or slightly less than that for 900 °C, and their length is ∼1500 nm, indicating an equal or larger surface-to-volume ratio for the 950 °C sample compared to the 900 °C sample. This correlation is consistent across a wide number of samples.

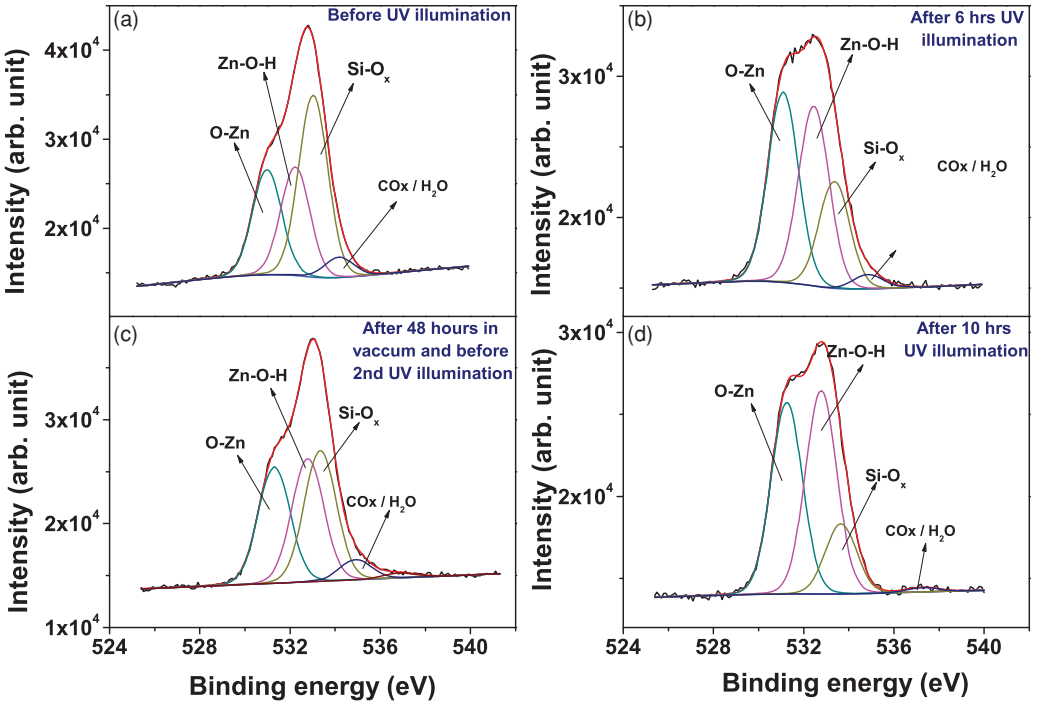

FIG. 4. (Color online) Peak fitted XPS O 1*s* spectra at different stages of the illumination experiment. (a) Before illumination, (b) after 6 h illumination, (c) after leaving sample in vacuum for 48 h before second illumination, and (d) after 10 h illumination.

In Fig. 5(e), we show the 2θ-ω scan of a typical ZnO nanorod-nanowall sample grown at 900°C, and in Fig. 5(f) we show the 2θ-ω scan of a typical ZnO nanorod sample grown at 950 °C. In both Figs. 5(e) and 5(f), peaks corresponding to the ZnO (0002) reflection from the aligned nanostructures, the ZnO (0004) reflection [second order of (0002) peak], and the sapphire (11-20) reflection from the *a*-sapphire substrate are seen. In Fig. 5(e), however, the (10-11) peak is visible on a linear scale, while in Fig. 5(f) the (10-11) peak is only visible on a log scale [intensity 0.3% of the sapphire (11-20) peak], as shown in the inset of this figure. The PL spectra of the sample whose XRD is shown in Fig. 5(e) show a high-intensity SX peak as in Fig. 5(g), and PL spectra of the sample shown in Fig. 5(f) show a small SX peak, as in Fig. 5(h). We have studied a range of samples where the intensity of the SX peak is small, and we have found in all cases a correlation between a relatively weak or undetectable SX peak in low-temperature PL and the (10-11) XRD peak also being weak and only visible on a log scale. For samples with intense SX peaks, the (10-11) XRD peak is clearly visible on a linear intensity scale. TEM studies have also been undertaken on both nanorod-nanowall and nanorod morphology samples. In Figs. 5(i) and 5(j), TEM images of nanorod-nanowall samples grown at 900 °C only are shown, as these show the nanowall structures with clear evidence of extended planar structural defects, such as grain boundaries, where nanowall structures have coalesced with nanorods during growth. In contrast, most of the actual nanorods in both 900 and 950 °C grown samples are found to be free of such extended structural defects (data not shown).

IV. DISCUSSION

We will discuss the data presented above with regard to two main issues and make some more speculative suggestions at the end of this section. First, we will discuss the evidence for the surface nature of the SX peak emission and specifically whether the defect(s) responsible are crystal defects confined to the (sub-) surface region[19] or adsorbed surface species that can bind excitons in their vicinity. Secondly, we will discuss the chemical nature of the defects responsible. Finally, we will discuss the variety of other contributing factors that may influence the relative strength of the SX.

As discussed previously in the Introduction, the main evidence in the literature for the surface nature of the defect responsible for the SX emission has come from studies of the scaling of relative peak intensity with experimental conditions and nanostructure morphology.[2,6,10] However, a key question, namely whether the defect(s) responsible are crystal defects confined to the (sub-) surface region[19] or adsorbed surface species that can bind excitons in their vicinity, remains unanswered. The behavior of the SX peak after electrical voltage application, presented in Sec. III A, provides strong evidence for the latter possibility in our view. These measurements indicate that the locally applied voltage and/or electric current in the region of the nanostructures consistently and reproducibly affect the adsorbed species responsible for the SX PL emission, and that the changes can be fully recovered by reexposure to air in zero bias. The exact microscopic mechanism for the changes we observe is at present unclear. The absence of a bias polarity or substrate carrier-type dependence (and the absence of an effect for

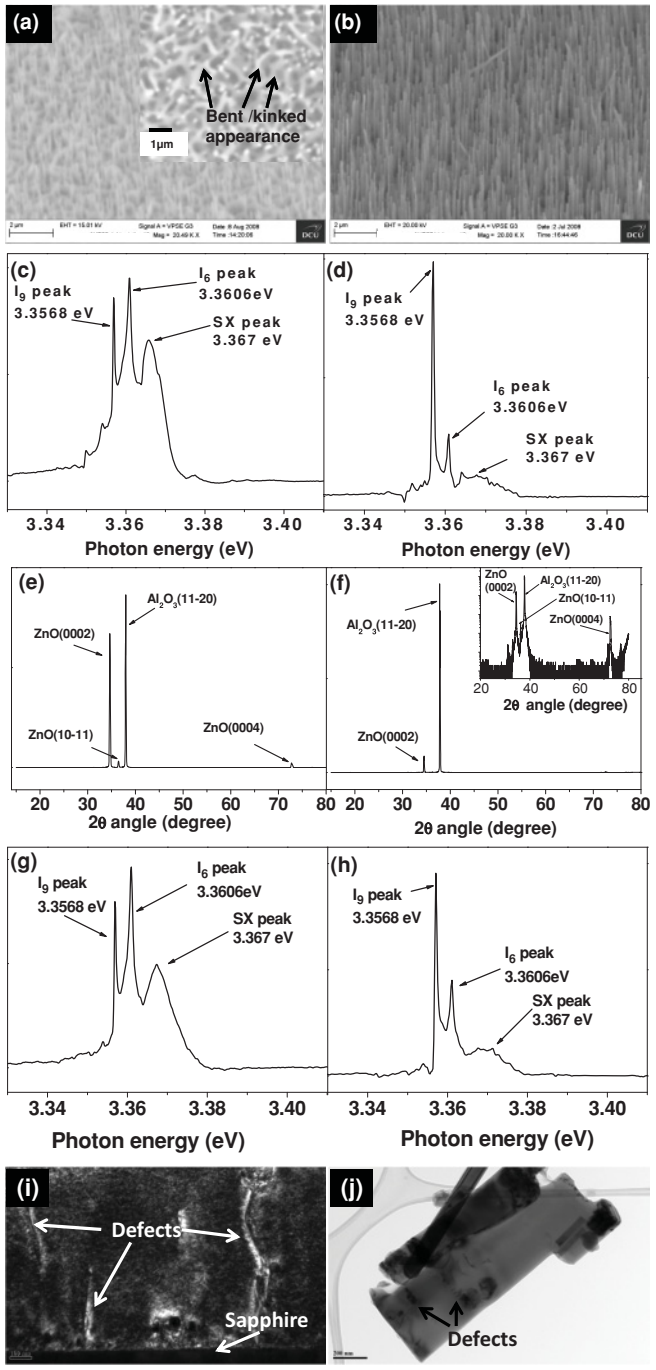

FIG. 5. SEM images (a) and (b) and PL spectra at 18 K (c) and (d) of ZnO nanorod-nanowall sample grown at 900 °C [(a) and (c)] and ZnO nanorod sample grown at 950 °C [(b) and (d)]. Inset of (a) shows plan view SEM image of ZnO nanorod-nanowall sample shown in (a). XRD 2θ-ω (e) and (f) and PL data (g) and (h) of sample grown at 900 °C [(e) and (g)] and sample grown at 950 °C [(f) and (h)]. Inset of (f) shows XRD 2θ-ω data of 950 °C grown sample on log scale. TEM images (i) and (j) of ZnO nanorod-nanowall samples grown at 900°C. (PL intensity scales are linear).

voltages less than 50 V) in the results points to localized heating effects due to the electric current, which may affect both the adsorbed species on nanostructures in the vicinity of the contact and also the silver paste used for contacting (which can release moisture or other chemical species). The consistent recovery seen indicates, however, that those heating effects do not lead to permanent effects due to sample annealing. Furthermore, it is also clear that voltage application has different effects in different atmospheres: in vacuum, it leads to an increase in the relative SX peak intensity, in air a reduction, and in a chemically inert ambient (He), no change is observed. The absence of any change in the inert He atmosphere suggests that the effect of the ambient may be to alter the density of available sites for adsorption of species (e.g., released by the heating effect of the current). Voltage application in vacuum may then lead to an uncompensated loss of a variety of weakly physisorbed species via desorption (uncompensated due to the low surrounding pressure), which then provides suitable accommodation sites for subsequent adsorption of the species responsible for the SX emission. In contrast, voltage application in air may lead to adsorption of species from the ambient, blocking suitable sites and perhaps even displacing some of the adsorbed species responsible for the SX emission. The stability of the samples during PL measurements in the cooled inert He gas is also consistent with these suggestions. The process of reexposure to air after voltage application, including warming up the sample from cryogenic to room temperature, has the effect of reversing any changes as the sample reequilibrates with the air ambient at room temperature. Furthermore, as mentioned above, discharging the electrical probes in the gas atmosphere leads to no change in the SX peak, so the possibilities of any charge state or depletion layer effects, which should follow the Fermi level position instantaneously, are also ruled out. In summary, the consistent variations and recovery at room temperature or below of the SX PL in these experiments (and on time scales where significant contributions from defect drift and diffusion in the sub-surface region are not possible) and with differing, but consistent and reproducible, behavior in different gas atmospheres provide strong evidence for the involvement of surface adsorbates in the SX PL emission as opposed to sub-surface crystal defects.

In terms of the chemical nature of the adsorbed species, which gives rise to the SX emission, as mentioned previously, species such as O_2^-, O^-, and O^{2-} have all been considered as possibilities. The two surface treatments of (a) plasma treatments and (b) UV illumination in high vacuum have both previously been shown to remove surface-adsorbed oxygen species such as O_2^-, O^- and O^{2-} (and indeed photolysis of the ZnO surface also occurs when UV light of energy greater than the band-gap energy is incident on ZnO samples in high vacuum).[21,22,38–43] Our plasma and UV illumination treatments use power densities and vacuum conditions similar to or better than most previous reports, and the experimental setups used in this study should be more than sufficient to desorb O/O_2 from the surface of ZnO nanostructures.[20,38,39,41,43–47] However, as reported in Secs. III B and III C above, the absence of any significant or consistent changes in the SX peak either following both O and Ar plasma treatments or after illuminating with UV light in high vacuum lead us to conclude that the SX is not due to adsorbed O/O_2 on the nanostructure surfaces.

The XPS data reported in Sec. III D clearly show that OH groups on the nanostructure surfaces are observed as strong and robust contributors to the spectra and are not removed

by UV illumination in vacuum. Furthermore, XPS studies after *in situ* annealing of this nanostructure sample up to 200 °C (performed after the series of UV exposures and related XPS measurements reported above) show no variation in the ZnO and OH signals (data not shown). This behavior shows how robust the OH contribution is, and it is consistent with a broader range of our studies on other ZnO nanorod, thin-film, and single-crystal samples, which have been annealed up to 1000 °C and exposed to cracked hydrogen at elevated temperatures (400 °C). These samples in all cases show no significant changes or reduction in the OH-related signal. Furthermore, the sample shown in Fig. 4, which exhibited intense SX PL, showed a stronger relative contribution from the OH XPS signal than other nanorod and planar samples. Thus, based on the XPS data reported in Sec. III D and Fig. 4, we find strong evidence for a relationship between the SX peak and the ubiquitous and robust OH-related adsorbed surface species. Previous work from our group, mentioned earlier in the Introduction, has shown that, with increasing temperature, the PL quenches strongly in samples that show a large SX peak,[7] due to increased nonradiative recombination with increasing temperature for these defects. There has also been a report that OH groups present on the surface of ZnO quantum dots are responsible for the quenching of band-edge excitonic emission.[48] Thus the high-temperature quenching of the PL of ZnO nanostructures that show strong SX emission at lower temperatures may be related to the presence of adsorbed OH species, which supports the assignment of such species as the microscopic origin of the SX peak.

Finally, it has been reported in the literature that the SX peak is the dominant peak for ultrathin nanowires of diameter less than 10 nm, and also that the SX peak intensity decreases with increasing nanowire-nanorod diameter within nonmonodisperse ensembles of morphologically similar nanostructures with a $(\text{diameter})^{-1}$ scaling relation; the SX peak has been attributed to a surface-related defect with intensity determined solely or mainly by the surface-to-volume ratio on these bases alone.[2,3,6,10,17] However, a number of reports of low-temperature PL from ZnO nanostructures with varying aspect ratios show no consistent correlation from one report to another between the SX peak relative intensity and the nanostructure aspect ratio; see e.g., Refs. 23–25. Furthermore, even within single reports, slightly different morphologies in an ensemble of nanostructures show considerable differences in the relative SX peak emission strength (such as the different morphologies A, B, and C referred to in Ref. 17 and the different morphologies referred to in the discussion of Fig. 1 of Ref. 2). Based on the entirety of these reported data, we question whether the SX peak's relative intensity is solely or mainly determined only by the nanostructure surface-to-volume ratio. Clearly, the fact that the defect responsible is a surface-related defect (most probably surface-adsorbed OH based on the discussion above) means that within nonmonodisperse ensembles of morphologically similar nanostructures, the diameter (or surface-to-volume ratio) will be the main determinant. However, the variations referred to above mean that other aspects of the crystallinity or morphology must also be important and may be crucial when considering different morphologies within an ensemble or structures from different laboratories.

From our studies reported in Sec. III E above, based on our observations of many samples grown at both 900 and 950 °C, we conclude that the relative intensity of the SX peak is not solely dependent on the surface-to-volume ratio of the ZnO material. In addition, the XRD data indicate a different alignment of a fraction of the ZnO nanostructured deposit for samples with nanorod-nanowall morphologies, which correlates with the SX peak emission intensity. Based on the relative intensities of the XRD peaks, this fraction is likely to be small in terms of overall volume, but it may slightly affect the alignment of subsequent nucleation and growth of primarily (0001)-textured material leading to different regions of deposit with slightly differing crystallite orientations. This crystalline misalignment will lead to planar defects such as grain boundaries at the regions of coalescence of the differently aligned regions as growth proceeds and will influence, we believe, especially the coalescence of nanowall structures with nanorod bases. Planar defects of this type are in fact seen in the wall structures using TEM, as in Figs. 5(i) and 5(j).

Based on these data, the relative intensity of the SX peak is strongly affected by the details of the nanostructure morphology and crystal quality, beyond effects solely attributable to the surface-to-volume ratio. Strong SX emission is seen in the nanorod-nanowall morphology samples and correlates with the (10-11) XRD peak strength. We believe that these factors are important in understanding the strong SX emission. First, the nanowall morphology displays a significantly bent or kinked appearance in plan view [shown in the inset of Fig. 5(a)] and these kink sites may offer a high density of attractive adsorption sites for OH species. Secondly, the presence of planar defects referred to above may also offer a high density of attractive adsorption sites for OH species at the regions where such defects intersect the nanostructure surfaces. Furthermore, adsorption may also occur at crystallite surfaces during nanostructure growth but prior to nanorod-nanowall coalescence, leading to trapped OH species at such planar defects. The variety of slightly differing surface adsorption sites may also readily explain the generally observed large width (∼5 meV) of the SX PL emission peak. There is evidence in support of this in the literature, including reports of low-temperature PL from ZnO nanostructures with varying aspect ratios, which show no consistent correlation from one report to another between the SX peak relative intensity and the nanostructure aspect ratio (as well as variations with morphology variations seen within individual reports); see e.g., Refs. 17 and 23– 25.

V. CONCLUSIONS

The microscopic origins of the SX peak have been studied by low-temperature PL in combination with various surface treatment methods, in addition to XRD, SEM, and TEM. Voltage application in high vacuum, air, and He gas show significant, consistent, and recoverable changes in the peak intensity in the different gas atmospheres, providing clear evidence that the defects responsible are adsorbed surface species. High vacuum UV illumination and plasma treatments show no consistent or reproducible changes in the SX emission intensity, and we conclude that O/O_2 is not the species

responsible for the SX peak in ZnO nanostructure PL. XPS data show it is very difficult to remove the ubiquitous adsorbed OH species, and that such species are strong candidates to be the origin of the SX emission. XRD, SEM, and TEM data show that the nanostructure morphology affects SX emission in a way not solely attributable to the surface-to-volume ratio.

Our final conclusion is that the SX peak is due to an exciton bound at the ZnO surface modified by an adsorbate, most likely an OH-related species, and that the SX signal is strongly affected by the detailed nanostructure morphology. This work contributes to the understanding of the SX emission in ZnO nanostructures, which is an important issue in terms of device applications given the association of this emission with PL quenching at higher temperatures.

ACKNOWLEDGMENTS

M.B., E.McG., G.H., K.K., and M.O.H. acknowledge financial support from an SFI-RFP grant (06/RFP/PHY052). H.K.K. and Y.S.J. acknowledge financial support from NSF Grants (No. DMR 0216785 and No. ECCS 0403865). We are pleased to acknowledge the assistance of Dr. Ram Prasad Gandhiraman, who grew 500 nm SiO_2 layers on Si substrates via PE-CVD.

*mahua.biswas2@mail.dcu.ie.

[1] B. K. Meyer, H. Alves, D. M. Hofmann, W. Kriegseis, D. Forster, F. Bertram, J. Christen, A. Hoffmann, M. Straßburg, M. Dworzak, U. Haboeck, and A. V. Rodina, Phys. Status Solidi B **241**, 231 (2004).

[2] L. Wischmeier, T. Voss, I. Ruckmann, J. Gutowski, A. C. Mofor, A. Bakin, and A. Waag, Phys. Rev. B **74**, 195333 (2006).

[3] D Stichtenoth, C Ronning, T Niermann, L Wischmeier, T Voss, C.-J. Chien, P.-C. Chang, and J. Grace Lu, Nanotechnology **18**, 435701 (2007).

[4] O. Brandt, C. Pfüller, C. Chèze, L. Geelhaar, and H. Riechert, Phys. Rev. B **81**, 045302 (2010).

[5] J.-P. Richters, T. Voss, L. Wischmeier, I. Ruckmann, and J. Gutowski, Appl. Phys. Lett. **92**, 011103 (2008).

[6] Y. Yang, B. K. Tay, X. W. Sun, J. Y. Sze, Z. J. Han, J. X. Wang, X. H. Zhang, Y. B. Li, and S. Zhang, Appl. Phys. Lett. **91**, 071921 (2007).

[7] J. Grabowska, A. Meaney, K. K. Nanda, J. P. Mosnier, M. O. Henry, J. R. Duclere, and E. McGlynn, Phys. Rev. B **71**, 115439 (2005).

[8] V. V. Travnikov, A. Freiberg, and S. F. Savikhin, J. Lumin. **47**, 107 (1990).

[9] J. P. Richters, T. Voss, D. S. Kim, R. Scholz, and M. Zacharias, Nanotechnology **19**, 305202 (2008).

[10] T. Voss and L. Wischmeier, J. Nanosci. Nanotechnol. **8**, 228 (2008).

[11] R. Tenne, V. M. Nabutovsky, E. Lifshitz, and A. F. Francis, Solid State Commun. **82**, 651 (1992).

[12] V. V. Travnikov, J. Cryst. Growth **101**, 579 (1990).

[13] V. V. Travnikov, JETP Letters **40**, 1060 (1984).

[14] G. J. Lapeyre and J. Anderson, Phys. Rev. Lett. **35**, 117 (1975).

[15] L. Wischmeier, T. Voss, I. Ruckmann, and J. Gutowski, Nanotechnology **19**, 135705 (2008).

[16] Y. Z. Zhang, H. P. He, Y. Z. Jin, B. H. Zhao, Z. Z. Ye, and H. P. Tang, J. Appl. Phys. **104**, 103529 (2008).

[17] L. Wischmeier, T. Voss, S. Börner, and W. Schade, Appl. Phys. A **84**, 111 (2006).

[18] T. Voss, J. P. Richters and A. Dev, Phys. Status Solidi B **247**, 2476 (2010).

[19] H. Jin Fan, A. S. Barnard, and M. Zacharias, Appl. Phys. Lett. **90**, 143116 (2007).

[20] J. Lagowski, J. E. S. Sproles, and H. C. Gatos, J. Appl. Phys. **48**, 3566 (1977).

[21] D. R. I. Bickley, P. G. Heiland, D. W. Hirschwald, D. E. Thull, P. F. Steinbach, M. R. Harborth, D. W. Bauer, P. A. Hausmann, D. A. J. Tench, P. J. Cunningham, P. M. W. Roberts, D. T. B. Grimley, P. D. Menzel, and P. H. P. Boehm, Faraday Discuss. Chem. Soc. **58**, 175 (1974).

[22] F. Steinbach and R. Harborth, Faraday Discuss. Chem. Soc. **58**, 143 (1974).

[23] H. Zhou, J. Fallert, J. Sartor, R. J. B. Dietz, C. Klingshirn, H. Kalt, D. Weissenberger, D. Gerthsen, H. Zeng, and W. Cai, Appl. Phys. Lett. **92**, 132112 (2008).

[24] Y. Li, M. Feneberg, A. Reiser, M. Schirra, R. Enchelmaier, A. Ladenburger, A. Langlois, R. Sauer, K. Thonke, J. Cai, and H. Rauscher, J. Appl. Phys. **99**, 054307 (2006).

[25] M. A. Reshchikov, A. Behrends, A. Bakin, and A. Waag, J. Vac. Sci. Technol. **27**, 1688 (2009).

[26] J. Grabowska, K. K. Nanda, E. McGlynn, J. P. Mosnier, and M. O. Henry, Surf. Coat. Technol. **200**, 1093 (2005).

[27] M. Biswas, E. McGlynn, M. O. Henry, M. McCann, and A. Rafferty, J. Appl. Phys. **105**, 094306 (2009).

[28] J. F. Moulder, W. F. Stickle, P. E. Sobol, and K. D. Bomben, *Handbook of X-Ray Photoelectron Spectroscopy*, 1st ed. (Perkin-Elmer Corp., Eden Prairie, MN, 1992).

[29] C. Wöll, Prog. Surf. Sci. **82**, 55 (2007).

[30] [http://srdata.nist.gov/xps/].

[31] O. Lupan, L. Chow, G. Chaic, B. Roldan, A. Naitabdi, A. Schulte, and H. Heinrich, Mater. Sci. Eng. B **145**, 57 (2007).

[32] C. D. Wagner and G. E. Muilenberg, *Handbook of X-ray Photoelectron Spectroscopy* (Perkin-Elmer Corp., Eden Prairie, MN, 1979).

[33] D. Elizabeth Pugel, R. D. Vispute, S. S. Hullavarad, T. Venkatesan, and B. Varughese, Appl. Surf. Sci. **254**, 2220 (2008).

[34] T. L. Barr, J. Phys. Chem. **82**, 1801 (1978).

[35] R.-D. Sun, A. Nakajima, A. Fujishima, T. Watanabe, and K. Hashimoto, J. Phys. Chem. B **105**, 1984 (2001).

[36] N. Asakuma, T. Fukui, M. Toki, K. Awazu, and H. Imai, Thin Solid Films **445**, 284 (2003).

[37] N. Asakuma, H. Hirashima, T. Fukui, M. Toki, K. Awazu, and H. Imai, Jpn. J. Appl. Phys. **41**, 3909 (2002).

[38] D. H. Zhang, J. Phys. D: Appl. Phys. **28**, 1273 (1995).

[39] J. Cunningham, E. Finn, and N. Samman, Faraday Discuss. Chem. Soc. **58**, 160 (1974).

[40] C. Jin, A. Tiwari, and R. J. Narayan, J. Appl. Phys. **98**, 083707 (2005).

[41] K. Keem, H. Kim, G.-T. Kim, J. S. Lee, B. Min, K. Cho, M.-Y. Sung, and S. Kim, Appl. Phys. Lett. **84**, 4376 (2004).

[42]D. C. R. Brundle, D. S. Evans, P. M. W. Roberts, D. D. Briggs, D. J. C. Fuggle, P. D. Menzel, D. F. R. Smith, P. J. M. Thomas, D. D. E. Parry, D. A. M. Bradshaw, D. P. Biloen, D. E. W. Plummer, D. T. B. Grimley, D. D. R. Lloyd, D. R. W. Joyner, D. J. Küppers, and D. H. Killesreiter, Faraday Discuss. Chem. Soc. **58**, 125 (1974).

[43]M. Liu and H. K. Kim, Appl. Phys. Lett. **84**, 173 (2004).

[44]Q. H. Li, T. Gao, Y. G. Wang, and T. H. Wang, Appl. Phys. Lett. **86**, 123117 (2005).

[45]E. Veuhoff and D. Kohl, J. Phys. C **14**, 2395 (1981).

[46]H. Kind, H. Yan, B. Messer, M. Law, and P. Yang, Adv. Mater. **14**, 158 (2002).

[47]S. A. Studenikin and N. Golego, J. Appl. Phys. **87**, 2413 (2000).

[48]H. Zhou, H. Alves, D. M. Hofmann, W. Kriegseis, B. K. Meyer, G. Kaczmarczyk, and A. Hoffmann, Appl. Phys. Lett. **80**, 210 (2002).